CARBON 47 (2009) 1028–1033

available at www.sciencedirect.com

ScienceDirect

journal homepage: www.elsevier.com/locate/carbon

Formation of endohedral Ni@C60 and exohedral Ni–C60 metallofullerene complexes by simulated ion implantation

*Erik C. Neyts**, *Annemie Bogaerts*

Research Group PLASMANT, Dept. Chemistry, University of Antwerp, Universiteitsplein 1, 2610 Antwerp, Belgium

ARTICLE INFO

Article history:
Received 1 August 2008
Accepted 5 December 2008
Available online 24 December 2008

ABSTRACT

The interaction of thermal and hyperthermal Ni ions with gas-phase C_{60} fullerene was investigated at two temperatures with classical molecular dynamics simulations using a recently developed interatomic many-body potential. The interaction between Ni and C_{60} is characterized in terms of the Ni–C_{60} binding sites, complex formation, and the collision and temperature induced deformation of the C_{60} cage structure. The simulations show how ion implantation theoretically allows the synthesis of both endohedral Ni@C_{60} and exohedral Ni–C_{60} metallofullerene complexes.

1. Introduction

Since their discovery in 1985 [1], metallofullerenes have attracted much attention because of their unique physical and chemical properties and potential applications, e.g. as electronic, optic and magnetic materials, as well as magnetic resonance imaging contrast agents and radiotracers in medical sciences [2–4]. Although most attention is devoted to endohedral metallofullerenes, (see e.g. Reference [5] and references therein), exohedral [6,7] and heterohedral [8] metallofullerenes have also been studied. Endohedral metallofullerenes are commonly produced by a DC electric arc discharge or a laser furnace method [5], although for the production of endohedral fullerenes in high purity, ion implantation may be a process to be attempted, both for noble gases [9] and metals [10–12]. In this process, the atoms to be encapsulated are ionized, accelerated, and implanted in the fullerene target.

While many authors have reported on the formation of metallofullerene complexes using rare earth metals and alkali and alkaline earth metals (e.g. Li, Be [13]; lanthanides, Ca, Sr, Ba, Sc, Ti, Y [5]; Th, Pa [14]; Cs [12]), the first-row transition metals have received far less attention [5,15,16]. Experimentally, the exohedral Ni–C_{60} and the substitutional Ni–C_{59} complex were reported on by Branz et al. [17] and Kong et al. [18,19]. The structure of the substitutional Ni–C_{59} complex and the endohedral Ni@C_{60} complex were reported on in simulation papers by Sparta et al. [20] and Alemany et al. [21], respectively. To the authors' knowledge, however, only one group has previously reported on the possible gas-phase synthesis of an endohedral Ni containing fullerene [22]. In this contribution, we demonstrate how molecular dynamics (MD) simulations predict the formation of both endohedral (Ni@C_{60}) and exohedral (Ni–C_{60}) metallofullerene complexes by ion implantation.

2. Simulation setup

Molecular dynamics simulations were carried out using a recently developed reactive interatomic Ni–C many-body potential [23]. The system is evolved in time using a symplectic velocity verlet integrator [24]. The time step was set to 0.1 fs to ensure energy conservation in the simulations to at least 2×10^{-4}%.

The simulation procedure was as follows. First, the C_{60} molecule was heated for 8×10^5 time steps to the desired temperature using the Andersen heat bath [25] in order to obtain the correct canonical temperature and atomic velocity distributions. This structure was then relaxed under NVE condi-

* *Corresponding author:* Fax: +32 3 820 23 76.
E-mail address: erik.neyts@ua.ac.be (E.C. Neyts).
0008-6223/$ - see front matter
doi:10.1016/j.carbon.2008.12.023

tions for 2×10^5 time steps. The resulting configuration was used as input configuration for the ion impact simulations. Two temperatures were considered: 300 and 2273 K, the latter corresponding to an arc discharge temperature [26]. At each temperature, one simulation was carried out with thermal Ni impacts, and 10 simulations were performed with Ni ion impact energies ranging from 10 to 100 eV with a uniform energy spacing of 10 eV. Each simulation consisted of 100 impacts, corresponding to in total 1100 ion impacts at each temperature.

Prior to each impact, the C_{60} molecule was randomly rotated around its center of mass. The hyperthermal Ni ions with energies 10–100 eV were allowed to impact with incidence normal to the projected {x,y} plane of the relaxed C_{60} molecule with random {x,y} position and {z} position beyond the cut-off of the potential (3.0 Å). This ensures the correct half-circle probability distribution for the incoming ion hitting any specific C_{60} target atom. The Ni atoms with thermal energy, on the other hand, were allowed to impinge under a random angle with a velocity taken from a Maxwell distribution corresponding to the gas-phase temperature, ensuring the correct spherically uniform impingement probability distribution. The initial minimum distance from the Ni atom to the nearest C-atom of the target was set equal to the cut-off of the potential.

3. Ni–C_{60} binding characteristics

Our simulations predict that the Ni–C_{60} interaction can be characterized by three regimes, depending on the ion impact energy. These regimes are exemplified in Fig. 1 and demonstrated in Fig. 2. Fig. 2 shows the different calculated fractions of NiC_{60} complexes. Note, however, that the total probability of NiC_{60} complex formation decreases from 1 at the lowest ion energies to about 0.4–0.5 at the highest ion energies.

(a) *First regime* – The first regime occurs at low (thermal up to 10 eV) impact energies, as indicated in Fig. 2 by area I. In this regime, only the formation of the exohedral Ni–C_{60} complex is observed. The Ni binds in all cases to either all five atoms of a pentagon or to all six atoms of a hexagon on the outer surface of the C_{60} with five or six bonds, respectively. At 300 K, the average C–Ni bond energy is −1.38 eV when the Ni binds to a pentagon, and −1.21 eV when the Ni binds to a hexagon. These values decrease to −1.32 eV and −1.15 eV, respectively, at a temperature of 2273 K. The location of the Ni is (on average) precisely in the center of the polygon, at an average normal distance of 1.52 Å above the pentagons and 1.38 Å above the hexagons at 300 K and a bit further, i.e. at 1.56 and 1.45 Å above the pentagons and hexagons, respectively, at 2273 K. Note that these binding configurations correspond to DFT-optimized geometries recently obtained for other exohedral metallofullerene complexes [7]. DFT calculations have also been carried out on Ni–C_{60} [21,27]. The Ni–C bond distances are in reasonable agreement

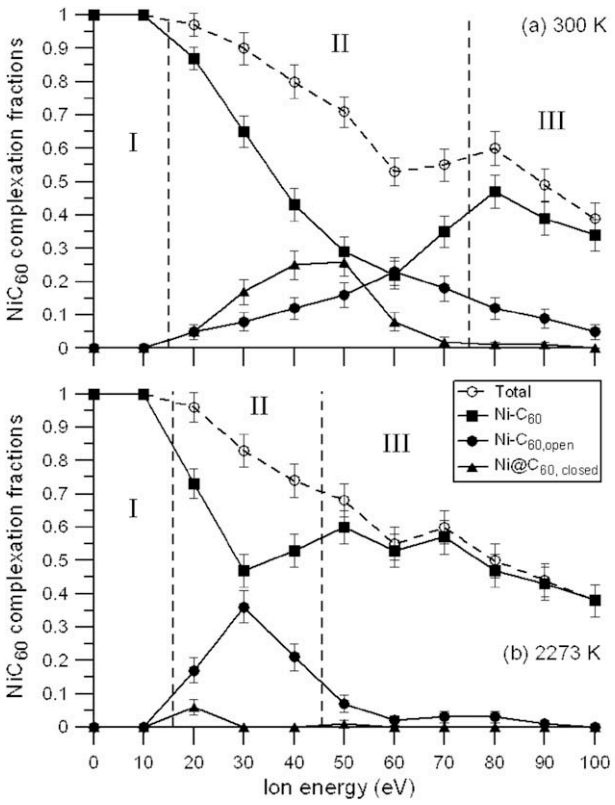

Fig. 2 – Calculated total complexation frequency, and frequencies of exohedral complexation, endohedral complexation in a closed cage, and endohedral complexation in an open cage, at a temperature of (a) 300 K and (b) 2273 K. The errors are calculated as the unbiased estimates of the standard deviation corresponding to a binomial distribution.

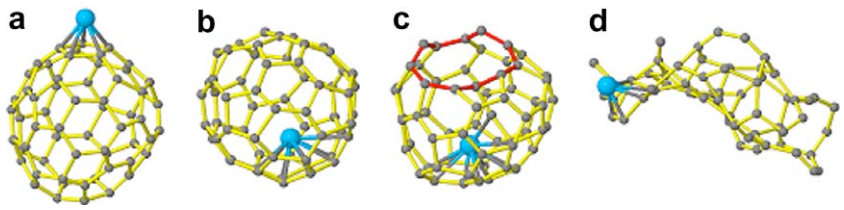

Fig. 1 – Typical calculated structures of Ni-fullerene complexes after Ni impacts with various energies: (a) thermal (resulting in an exohedral complex); (b) 30 eV (yielding an endohedral complex with closed cage); (c) 60 eV (endohedral complex with open cage); (d) 90 eV (Ni attached to damaged carbon network), exemplifying the different Ni–C_{60} interaction regimes found in the simulations. The blue atom is Ni, the grey atoms are C, and the red bonds in panel (c) trace the circumference of a collision induced nonagon orifice. (For interpretation of the references to colour in this figure legend, the reader is referred to the web version of this article.)

(2.01 Å in this work vs. 2.15 Å in Reference [21] for Ni-on-hexagon, and 1.97 Å vs. 2.13 Å for Ni-on-pentagon), taking into account that the values given in Reference [21] correspond to optimized geometries, while our values correspond to average bond lengths as the simulation evolves dynamically. Furthermore, other *ab initio* calculations [27] on Ni–C_{60} predicted Ni–C bond lengths up to 0.15 Å shorter than those reported in Reference [21], as well as different most stable geometries. Finally, the calculated average C–C bond lengths in this work of 1.44 Å are in excellent agreement with both a DFT value [21] of 1.45 Å and the experimental value [28] of 1.44 Å.

While the ratio of the total area of the pentagons to the total area of the hexagons on C_{60} is about 0.4, we find the ratio of Ni sticking to a pentagon to Ni sticking to a hexagon to be about 0.85 at 300 K and 0.65 at 2273 K, in the case of thermal impacts, and about 0.3 in the case of 10 eV impacts at both temperatures. This discrepancy between the area covered by pentagons and hexagons, and the observed sticking ratio, results from the shorter C_1–C_3 distance in a pentagon compared to this distance in a hexagon. Indeed, when the Ni ion forms its first two bonds with the C_{60}, the two C-atoms belong either to a 6:6 bond (i.e. a bond shared between two hexagons), or to a 6:5 bond (i.e. a bond shared between a hexagon and a pentagon) (see Fig. 3). In the case of a 6:6 bond, the C-atom closest to the Ni atom (and hence, the next atom in time with which the Ni will interact), will be part of the same hexagon as the two C-atoms forming the 6:6 bond, and hence, the Ni will bind to that hexagon. In case of a 6:5 bond, however, the closest C-atom to react with will always be part of a pentagon (quadruplet of atoms Ni–C_1–C_2–$C_{3,p}$ in Fig. 3). If the ion has time to adjust its position to the potential energy field of the third carbon atom, then the quadruplet Ni–C_1–C_2–$C_{3,h}$ will never be formed, since the distance Ni–$C_{3,h}$ is larger than the distance Ni–$C_{3,p}$ by about 0.35 Å. The ratio of the number of sticking events on a pentagon vs. on a hexagon therefore, depends on the ratio of the number of 6:5 bonds and the number of 6:6 bonds.

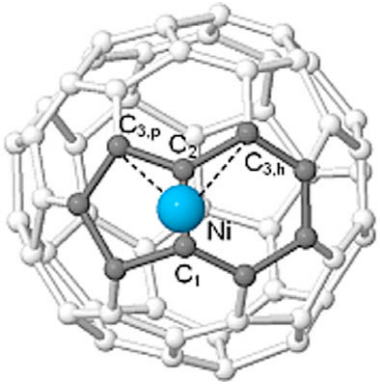

Fig. 3 – Representation of the interaction distance separating the incoming Ni ion and a carbon belonging to either a pentagon ($C_{3,p}$) or a hexagon ($C_{3,h}$). In this figure, the Ni is already bound to carbon atoms C_1 and C_2. The distance Ni–$C_{3,p}$ is always shorter than the distance Ni–$C_{3,h}$. Note that this configuration is only found as an intermediate to either Ni–C_{3h} or Ni–C_{3p} configurations.

Hence, there are two competing factors in determining the sticking ratio: (i) the larger surface area covered by the hexagons, and (ii) the higher number of 6:5 C–C bonds pulling the impinging Ni towards the nearest pentagon. The ratio of the areas covered by pentagons and hexagons is in C_{60} about 0.4, while the ratio of 6:5 bonds to 6:6 bonds is 2. The fraction of sticking events on a pentagon can therefore, be expected to be about 0.8, to be compared to our simulated sticking ratio of 0.85 at 300 K in the case of thermal impacts. Note that this prediction assumes that the incoming ion has enough time to adjust its position to the potential energy field as the first three C–Ni bonds are being formed. At a temperature of 2273 K, however, the Ni atom has less time to adjust its trajectory while approaching the C_{60} to the potential energy field (since it has higher kinetic energy), and the ratio of the fraction sticking on pentagon vs. sticking on hexagon is found to be 0.65, closer to the ratio of the areas covered by pentagons and hexagons. At an ion impact energy of 10 eV, the ion will not have time at all to adjust its position according to the potential energy field of the third C-atom, and the sticking ratio will be determined mostly by the surface area covered.

(b) *Second regime* – The second Ni–C interaction regime is found at medium ion impact energies, ranging from 20 to about 70 eV at 300 K, and from 20 to about 40 eV at 2273 K. This regime is indicated in Fig. 2 by area II. Here, one of three complex formation processes may happen:

(IIa) the Ni ion binds to the outer surface of the C_{60} (i.e. formation of the exohedral Ni–C_{60} complex, corresponding to the first regime);
(IIb) the ion breaks open the cage structure, binds to the inner surface of the C_{60} and the cage closes again (i.e. formation of the endohedral Ni@$C_{60,\text{closed complex}}$);
(IIc) the ion enters the cage structure, binds to the inner surface of the C_{60} but the cage remains open (i.e. formation of the endohedral Ni@$C_{60,\text{open complex}}$).

These three processes are complemented by two additional phenomena; i.e. the ion is not binding to the carbon network at all, and the collision induced damaging of the C_{60} cage structure. Both processes occur at all ion energies, but with increasing probability for higher ion energy. Indeed, as can be deduced from Fig. 2, the probability that the ion does not bind to the C_{60} (relative to the total number of impacts at a given energy) increases from nearly zero at 20 eV to 0.40 at 70 eV in the case of 300 K and to 0.25 at 40 eV, in the case of 2273 K. The collision induced damage will be discussed in Section 4.

Examples of resulting closed and open configurations are shown in Fig. 1b and c, respectively. Our simulations show that in the case of Ni@C_{60} formation, the Ni atom is strongly off-center, and strongly bound to the carbon network, as is also observed experimentally in endohedral metallofullerenes [5].

At 300 K, our calculations predict that the probability of closed and open Ni@C_{60} formation is quite comparable, but the probability of closed cage formation is a bit higher at low-

er impact energies, whereas at higher impact energies, more open cages are created, as can be deduced from Fig. 2a. At 2273 K, the formation of the $Ni@C_{60,closed}$ was observed only in a few cases (see Fig. 2b). Note that we define the structure to be "open" if at least one ring in the structure was a nonagon (or larger ring), as illustrated in Fig. 1c. This choice was made because the circumradius of a nonagon corresponds to the sum of the inner radii of C and Ni, hence, allowing the Ni to escape from the cage much more easily compared to escape through an octagon. Note, however, that this is a somewhat arbitrary criterion, in spite of the argument given.

The energy dependence of the $Ni@C_{60,closed\ cage}/Ni@C_{60,open\ cage}$ ratio can be explained as follows. When the energy is above the threshold to break at least 1 C–C bond, the ion can enter the cage through the collision induced orifice. The network itself, however, is not much damaged, and can still heal itself, thereby regenerating the original cage structure. On the other hand, the number of C–C bonds broken during the collision stage increases with rising ion energy, and so does the probability that a Ni ion will enter the cage. If, however, the ion energy becomes so large that the carbon network becomes too damaged to heal itself, the number of open cages will overtake the number of closed cages. As the ion energy keeps on increasing, this process continues, and switches to the third regime (see below).

Also the nature of the Ni–C interactions is observed to be energy dependent. At medium-low kinetic energies (10–30 eV), the observed bond breaking mechanism is of a chemical nature, i.e. the ion has enough kinetic energy to force itself through a hexagon or pentagon, thereby pulling apart covalently bound C-atoms by virtue of the repulsive part of the potential energy function. This mechanism bears a strong resemblance to the so-called 'swift chemical sputtering' mechanism observed by Nordlund et al. [29] and Salonen et al. [30] for amorphous carbon systems. At higher kinetic energies, this mechanism is complemented by a collision induced physical displacement of individual C-atoms, leading to an increasing number of broken C–C bonds.

At still higher energies, the latter process is further enhanced resulting in sputtering of C-atoms from the C_{60} network. Note that the displacement energy of carbon in graphite is about 35 eV [31]. Consider the kinematic factor $T_{12} = 4M_1M_2/(M_1 + M_2)^2$, where M_1 and M_2 are the masses of the collision partners. For the combination Ni–C, this factor is about 0.56. Hence, the impinging Ni ion must have at least 62.5 eV in order to physically sputter a C-atom from the C_{60} molecule. This defines the transition to the third regime where destruction of the network becomes important.

(c) *Third regime* – The third regime occurs at the highest energies investigated, starting from about 70 eV at 300 K, and from about 50 eV at 2273 K, as indicated in Fig. 2a and b by area III. As can be expected, the ion has now so much kinetic energy, that it often does not bind to the C_{60} molecule, and nearly always severely damages the cage structure. If it binds, it does not form a true exohedral Ni–C_{60} complex, due to the strong deformation of the structure. Indeed, for a kinematic factor of 0.56, a Ni ion impinging with 100 eV can transfer up to 56 eV to a carbon atom, which leads to two energetic species: a C-atom with 56 eV (or less), and a Ni atom with 44 eV (or more). These species can further transfer their energy to other carbon atoms by subsequent collisions. Hence, a cascade of energetic atoms is created, each having enough kinetic energy to break an additional bond, thereby destroying the network structure. In more than half of the cases, the Ni ion retains enough kinetic energy such that it does not remain bonded to the network, but rather escapes, as is again clear from Fig. 2.

4. Cage deformation

Due to both the thermal vibrations of the C_{60} cage and the energetic impacts of the nickel on the C_{60}, the spherical C_{60} cage structure will be deformed. The resulting asphericity of the carbon network can be quantified by the relative shape anisotropy Ω. Consider the tensor of gyration [32]:

$$S_{m,n} = \frac{1}{N}\sum_{i\in C} r_m^{(i)} r_n^{(i)} \tag{1}$$

where $r_m^{(i)}$ denotes the mth Cartesian coordinate of the ith carbon atom out of a collection of N particles, and where the origin of the coordinate system resides at the system center of mass. Using an orthogonal transformation, the tensor $\mathbf{S}$ can be diagonalized to form a diagonal matrix with the three eigenvalues $\lambda_1^2 \leqslant \lambda_2^2 \leqslant \lambda_3^2$ being the squared lengths of the principal axes of the gyration ellipsoid. The trace of the matrix defines the squared radius of gyration R_g. Further defining $b = \lambda_3^2 - \frac{1}{2}(\lambda_2^2 - \lambda_1^2)$ and $c = \lambda_2^2 - \lambda_1^2$, the relative shape anisotropy Ω is defined as [33]:

$$\Omega = \frac{b^2 + (3/4)c^2}{R_g^4} \tag{2}$$

The relative shape anisotropy is bounded to values between 0 and 1, where 0 corresponds to tetrahedral or higher symmetry, 0.25 to planar geometries and 1 to linear structures [33]. A perfect buckyball will therefore have $\Omega = 0.0$, and higher values of Ω indicate increasing deviation from the perfect spherical shape.

The evolution of the relative shape anisotropy for the carbon network as a function of the Ni impact energy is shown for both temperatures in Fig. 4a. The relative shape anisotropy is calculated as the average over all end configurations for the corresponding simulation condition. As can be seen from the figure, the carbon structure remains a nearly perfect sphere at thermal and medium–low energies, as exohedral Ni–C_{60} and later endohedral $Ni@C_{60}$ complexes are formed. The shape deformation becomes appreciable only at 50 eV in the case of 300 K, while at 2273 K a comparable value is already found at 20 eV. This observation can be related to Fig. 4b, showing the number of broken C–C bonds as a function of ion impact energy for both temperatures. Indeed, at 300 K, the C–C bonds are somewhat shorter and stronger compared to the situation at 2273 K, and the vibrational amplitude of the C–C bonds in C_{60} is about one order of magnitude smaller than at 2273 K. Hence, at 2273 K, the Ni ion can penetrate a C–C bond much more easily compared to the case of 300 K, resulting in the breaking up of more C–C bonds and in significant shape deformation at lower impact energies.

Comparing both figures, a near-linear relation between the number of broken C–C bonds and the relative shape anisotropy is found. Hence, while the relative shape anisotropy is

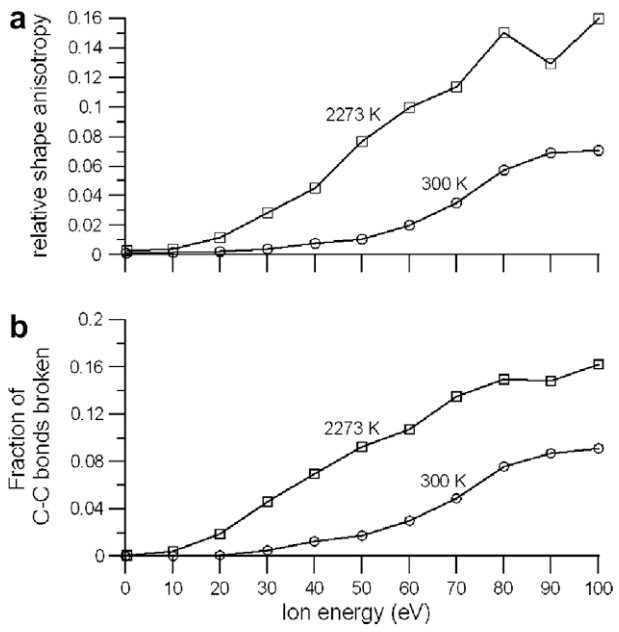

Fig. 4 – Calculated (a) relative shape anisotropy and (b) fraction of C–C bonds broken in the C_{60} molecule as a function of the ion impact energy.

not much influenced by the temperature itself (compare the values at both temperatures for thermal impacts), a high temperature does lead to more network damage by virtue of the ion impacts (see above), and as such, indirectly leads to a higher relative shape anisotropy.

Finally, regular oscillations in the relative shape anisotropy with a period of about 125 fs are found in the case of Ni–C_{60} complexation (i.e. mainly at low ion energies), while less regular oscillations (with respect to the amplitude) with a period of about 115 fs are found in the case of Ni@$C_{60,closed}$ (i.e. mainly at medium ion energies). In the case of strongly deformed networks (i.e. at high impact energies) no such oscillations were found.

5. Conclusion

We have investigated the theoretical formation of both exohedral Ni–C_{60} and endohedral Ni@C_{60} metallofullerene complexes by ion implantation using molecular dynamics simulations. It is shown how the impinging ion will bind to the outer surface of the C_{60} target at low energies, binds endohedrally by (temporarily) opening the cage structure at medium energies, and destroys the cage structure at high energy. At medium impact energies, an optimum value for the ion impact energy to generate endohedral Ni@C_{60} is found to be about 35–40 eV at 300 K. Finally, the deformation of the cage structure is found to be a function of both the ion energy and the temperature, enhancing the collision damage at high temperature. Our calculated results are in fair agreement with reported results from literature as far as comparison is currently possible. Therefore, as our simulations theoretically predict the possible synthesis of endohedral Ni@C_{60} by ion implantation, these results may lead to an increased experimental effort to synthesize these fascinating molecules.

Acknowledgments

E. Neyts acknowledges the FWO-Flanders (Fund for Scientific Research-Flanders) for financial support. The authors also gratefully acknowledge useful discussions with Prof. Y. Shibuta, financial support from the Prime Minister's Office through IAP VI, and calculation support of the core facility CALCUA, provided by the University of Antwerp.

REFERENCES

[1] Heath JR, O'Brian SC, Zhang Q, Liu Y, Curl RF, Tittel FK, et al. Lanthanum complexes of spheroidal carbon shells. J Am Chem Soc 1985;107(25):7779–80.
[2] Funasaka H, Sakurai K, Oda Y, Yamamoto K, Takahashi T. Magnetic-properties of Gd-at-C82 metallofullerene. Chem Phys Lett 1995;232(3):273–7.
[3] Wilson LJ. Medical applications of fullerenes and metallofullerenes. Interface. The Electrochemical Society; 1999. p. 24–8.
[4] Bakry R, Vallant RM, Najam-ul-Haq M, Rainer M, Szabo Z, Huck CW, et al. Medicinal applications of fullerenes. Int J Nanomed 2007;2:639–49.
[5] Shinohara H. Endohedral metallofullerenes. Rep Prog Phys 2000;63(6):843–92.
[6] Loboda O, Jensen VR, Borve KJ. Multiple additions of palladium to C-60. Fullerenes Nanotubes Carbon Nanostruct 2006;14(2–3):365–71.
[7] Lu G, Deng K, Wu H. Geometric and electronic structures of metal-substitutional fullerene C59Sm and metal-exohedral fullerenes C60Sm. J Chem Phys 2006;124(5):54305.
[8] Vostrowsky O, Hirsch A. Heterofullerenes. Chem Rev 2006;106:5191–207.
[9] Watanabe S, Ishioka NS, Sekine T, Osa A, Koizumi M, Shimomura H, et al. Production of endohedral Xe-133-fullerene by ion implantation. Radioanal Nucl Chem 2003;255(3):495–8.
[10] Kolodney E, Manor Y, Kaplan A, Bekkerman A, Tsipinyuk B. Impact formation of endohedral fullerenes at surfaces: comparing field-free yield measurements with model calculations. Int J Mass Spectrom 2006;249–250: 8–13.
[11] Gromov A, Ostrovskii D, Lassesson A, Jonsson M, Campbell EEB. Fourier transform infrared and Raman spectroscopic study of chromatographically isolated Li@C-60 and Li@C-70. J Phys Chem B 2003;107(41):11290–301.
[12] Kaplan A, Bekkerman A, Tsipinyuk B, Kolodney E. The formation and ejection of endohedral Cs@C-60(+) by low energy collisions (35–220 eV) of Cs+ ions with surface adsorbed C-60 molecules. J Chem Phys 2002;117(7): 3484–91.
[13] Ohtsuki T, Ohno K, Shiga K, Kawazoe K, Maruyama Y. Systematic study of foreign-atom-doped fullerenes by using a nuclear recoil method and their MD simulation. J Chem Phys 2000;112(6):2834–42.
[14] Akiyama K, Sueki K, Haba H, Tsukada K, Asai M, Yaita Y, et al. Production and characterization of actinide metallofullerenes. J Radioanal Nucl Chem 2003;255(1):155–8.
[15] Dresselhaus MS, Dresselhaus G, Eklund PC. Science of fullerenes and carbon nanotubes. San Diego: Academic Press; 1996. p. 132–33.
[16] Huang H, Ata M, Yoshimoto Y. Cu@C-60 formation in rf-plasma and ring-current induced magnetism of C-60. Chem Commun 2004(10):1206–7.

[17] Branz W, Billas IML, Malinowski N, Tast F, Heinebrodt M, Martin TP. Cage substitution in metal-fullerene clusters. J Chem Phys 1998;109(9):3425–30.
[18] Kong QY, Shen YF, Zhao L, Zhuang J, Qian SX, Li YF, et al. Formation of various types of metallofullerenes by laser ablation of externally doped fullerenes C60Mx (M = Sm, Pt, Ni, La, Y, and Rh). J Chem Phys 2002;116(1):128–36.
[19] Kong Q, Zhuang J, Li X, Cai R, Zhao L, Qian S, et al. Formation of metallofullerenes by laser ablation of externally doped fullerenes C60Mx (M = Sm, Pt and Ni). Appl Phys A-Mat Sci Proc 2002;75(3):367–74.
[20] Sparta M, Jensen VR, Borve KJ. Fullerenes, structure and stability of substitutional metallofullerenes of the first-row transition metals. Fullerenes Nanotubes Carbon Nanostruct 2006;14(2–3):269–78.
[21] Alemany MMG, Diéguez O, Rey C, Gallego LJ. A density-functional study of the structures and electronic properties of C59Ni and C60Ni clusters. J Chem Phys 2001;114(21):9371–4.
[22] Yamaguchi Y, Maruyama S. A molecular dynamics study on the formation of metallofullerene. Eur Phys J D 1999;9(1–4):385–8.
[23] Shibuta Y, Maruyama S. Bond-order potential for transition metal carbide cluster for the growth simulation of a single-walled carbon nanotube. Comp Mat Sci 2007;39(4):842–8.
[24] Swope WC, Anderson HC, Berens PH, Wilson KR. A computer-simulation method for the calculation of equilibrium-constants for the formation of physical clusters of molecules – application to small water clusters. J Chem Phys 1982;76(1):637–49.
[25] Andersen HC. Molecular-dynamics simulations at constant pressure and–or temperature. J Chem Phys 1980;72(4):2384–93.
[26] Kuznetsov VL, Usoltseva AN, Chuvilin AL, Obraztsova ED, Bonard JM. Thermodynamic analysis of nucleation of carbon deposits on metal particles and its implications for the growth of carbon nanotubes. Phys Rev B 2001;64(23):235401/1–7.
[27] Andriotis AN, Menon M. Geometry and bonding in small (C-60)(n)Ni-m clusters. Phys Rev B 1999;60(7):4521–4.
[28] Hedberg K, Hedberg L, Bethune DS, Brown CA, Dorn HC, Johnson RD, et al. Bond lengths in free molecules of buckminsterfullerene, c60, from gas-phase electron-diffraction. Science 1991;254(5030):410–2.
[29] Nordlund K, Salonen E, Keinonen J, Wu CH. Sputtering of hydrocarbons by ion-induced breaking of chemical bonds. Nucl Instrum Meth B 2001;180:77–84.
[30] Salonen E, Nordlund K, Keikonen J, Wu CH. Bond-breaking mechanism of sputtering. Europhys Lett 2000;52(5):504–10.
[31] Robertson J. Diamond-like amorphous carbon. Mat Sci Eng R 2002;37(4–6):129–281.
[32] Hellmann M, Weiss M, Heermann DW. Monte Carlo simulations reveal the straightening of an end-grafted flexible chain with a rigid side chain. Phys Rev E 2007;76(2):021802.
[33] Bosko JT, Todd BD, Sadus RJ. Analysis of the shape of dendrimers under shear. J Chem Phys 2006;124(4):044910.